

per second for the 100-nm diodes. The value for the 100-nm diodes is calculated directly from the optical image, where the diodes appear as 300-nm spots. If the diameter is assumed to be 100 nm, the number of photons per second increases by one order of magnitude to 10^2 . Looking at the quantum efficiencies established for large polymer LEDs in the family of polythiophenes, 0.1 to 1% external efficiencies, and current densities of 10 mA/cm^2 , we could expect 10^8 to 10^9 photons per second from the 10- μm LEDs and 10^4 to 10^5 photons per second from the 100-nm LEDs. Transmission losses in the metal electrode account for a part of this discrepancy and are measured by optical spectroscopy to be on the order of 60 to 80%. For our combination of materials, the quantum efficiency is most probably less than 0.1%, which, together with the transmission losses, brings the theoretical and experimental values into agreement with each other.

The numbers of emitted photons per second are calculated for the currents and voltages shown in the figures. It should be possible to increase these numbers by at least two orders of magnitude by increasing the current and using pulse techniques (21). As a comparison, it could be mentioned that one of the standard probes for SNOM, a tapered Al-coated optical fiber with a small aperture, suppresses the incoming light typically by a factor of 10^5 (8). Different techniques have been used with light intensities between 10^3 and 10^{11} photons per second for subwavelength light sources (22–24). We can then compare these results with projections of the best results for polymer nano-LEDs, where we may assume that we could increase efficiency to somewhere in the range of 1 to 10% and also that we might be able to operate the devices at current densities 10 times higher than those used presently. These developments would bring the photon emission up to the range of 10^7 to 10^8 photons per second, which puts the polymer nano-LEDs somewhere in the mid-range of the available techniques with respect to light intensity. Therefore, it should not be expected that polymer nano-LEDs would offer drastically better performance as subwavelength light sources than alternative devices. Rather, an advantage for the use of nano-LEDs may be in the ability to manufacture not one but thousands of light sources at the same time. This accomplishment might then be used to create efficient photopatterning processes that could be used to produce a large number of identical patterns simultaneously.

It may be possible in the future to improve a number of aspects of these structures—for instance, increasing the efficiency by using transport layers (20) or finding an appropriate transparent electron injector that could be used in this type of geometry.

The problem with heat expansion in the contacting polymer fibers could be reduced by using a much thinner insulating layer than the microfiltration membrane, in which small holes for polymerization could be made. The possibility of preparing thousands or millions of light sources at the same time, which is essential for some applications, may require methods such as ion-beam etching to control the distribution of light sources on the surface.

REFERENCES AND NOTES

1. J. H. Burroughes *et al.*, *Nature* **347**, 539 (1990).
2. D. Braun and A. J. Heeger, *Appl. Phys. Lett.* **58**, 1982 (1991).
3. G. Gustafsson *et al.*, *Nature* **357**, 477 (1992).
4. R. Friend, D. Bradley, A. Holmes, *Physics World* **1992**, 42 (1992).
5. M. Berggren *et al.*, *Nature* **372**, 444 (1994).
6. P. Dyreklev *et al.*, *Adv. Mater.*, in press.
7. I. D. Parker, *J. Appl. Phys.* **75**, 1656 (1994).
8. N. F. v. Hulst, M. H. P. Moers, B. Bölgel, *J. Microsc.* **171**, 95 (1993).
9. N. F. v. Hulst *et al.*, *Appl. Phys. Lett.* **62**, 461 (1993).
10. Q. Pei, G. Zuccarello, M. Ahlskog, O. Inganäs, *Polymer* **35**, 1347 (1994).

11. G. Heywang and F. Jonas, *Adv. Mater.* **4**, 116 (1992).
12. J. C. Gustafsson, B. Liedberg, O. Inganäs, *Solid State Ionics* **69**, 145 (1994).
13. M. Dietrich, J. Heinze, G. Heywang, F. Jonas, *J. Electrochem. Soc.* **369**, 87 (1994).
14. M. Berggren *et al.*, *J. Appl. Phys.*, in press.
15. Z. Cai and C. R. Martin, *J. Am. Chem. Soc.* **111**, 4138 (1989).
16. M. Granström and O. Inganäs, *Synth. Metals* **55–57**, 460 (1993).
17. Z. Cai, J. Lei, W. Liang, V. Menon, C. R. Martin, *Chem. Mater.* **3**, 960 (1991).
18. M. Granström and O. Inganäs, in preparation.
19. A. R. Brown *et al.*, *Chem. Phys. Lett.* **200**, 1 (1992).
20. A. R. Brown *et al.*, *Appl. Phys. Lett.* **61**, 2793 (1992).
21. D. Braun, D. Moses, C. Zhang, A. J. Heeger, *ibid.*, p. 3092.
22. N. Kuck, K. Lieberman, A. Lewis, A. Vecht, *ibid.*, p. 139.
23. A. Lewis and K. Lieberman, *Nature* **354**, 214 (1991).
24. E. Betzig, J. K. Trautman, T. D. Harris, J. S. Weiner, R. L. Kostelak, *Science* **251**, 1468 (1991).
25. We thank N. F. van Hulst and M. H. P. Moers for fruitful discussions. This work was supported by the Micronics program of the Swedish National Board for Industrial and Technical Development.

20 September 1994; accepted 19 December 1994

Influence of Lunar Phase on Daily Global Temperatures

Robert C. Balling Jr.* and Randall S. Cerveny

A newly available data set of daily satellite-derived, lower-tropospheric global temperature anomalies provides an opportunity to assess the influence of lunar phase on planetary temperature. These results reveal a statistically significant 0.02 K modulation between new moon and full moon, with the warmest daily global temperatures over a synodic month coincident with the occurrence of the full moon. Spectral analysis of the daily temperature record confirms the presence of a periodicity that matches the lunar synodic (29.53-day) cycle. The precision of the satellite-based daily temperature record allows verification that the moon exerts a discernible influence on the short-term, global temperature record.

Throughout history, many societies and individuals have believed that the moon exerts an influence on weather and climate. Indeed, scientists have been able to identify lunar-phase impacts on precipitation variations (1–4), thunderstorm frequency (5), ice nuclei concentrations (6), diurnal pressure changes (7), hurricanes (8), cloudiness as measured by sunshine recorders (9), and possibly global surface-temperature estimates (10). Adderley and Bowen (2, p. 749) claimed that “the appearance of a lunar component in daily temperature in certain parts of the world [is] comparatively well known” but is “extremely small and difficult to detect.” Until recently, the clear identification of a lunar influence on planetary temperature

was complicated by the lack of an accurate measure of global temperature on a daily basis.

A data set of significant reliability and sensitivity is now available that is potentially capable of being used to detect a lunar influence on global temperature. Spencer and Christy (11) have developed a lower-tropospheric (lowest 6 km) measure of global temperature based on microwave emissions of molecular oxygen. These microwave measurements are made by polar-orbiting satellites, thereby providing for coverage of the entire planet. The details of the measurement procedures are well documented, and this global data set is now widely used in climatic research (12–20). Although most scientists have used the monthly averaged, satellite-based temperature measurements, daily, globally averaged lower-tropospheric temperatures are now available (21,

Office of Climatology, Arizona State University, Tempe, AZ 85287, USA.

*To whom correspondence should be addressed.

22). In this investigation, we use these daily global temperatures to identify the lunar influence on planetary temperature.

The daily temperature record used in this study extends from 3 January 1979 to 31 August 1994. These daily data are expressed as global temperature anomalies calculated from a 1982–1991 base period when the lower-tropospheric temperature averaged ≈ 269 K; only 1.8% of the data are missing over the entire length of record. The daily temperature anomalies have a mean of -0.01 K (reflecting the global cooling after the 1991 eruption of Mount Pinatubo), have a standard deviation of 0.21 K, and range from -0.61 K on 2 August 1992 to 0.61 K on 29 December 1987.

We computed the lunar phase for each day coinciding with the planetary temperature record by determining the average angular difference between the apparent longitudes of the moon and sun for that day. The cycle of lunar-phase magnitudes varies from 0.0 for the new moon to 1.0 for the full moon; lunar phase variations define the lunar synodic cycle of 29.53 days.

Four different analytical procedures reveal the existence of a lunar influence on the daily lower-tropospheric global temperatures:

1) The global temperature anomalies were averaged within 14 lunar categories of approximately equal n size similar in nature to the categories used in earlier studies (1–4). A plot of the results (Fig. 1) reveals a strong linear relation between lunar phase and mean planetary temperature. The warmest daily temperatures over a synodic month are coincident with the occurrence of the full moon when temperature anomalies are generally 0.02 K higher than during new moon periods.

2) We further divided the temperature data into two lunar phase classes characterizing the extremes of the synodic month. A near-new moon class was defined as having lunar phase values < 0.10 , whereas a near-full moon class was confined to lunar phase

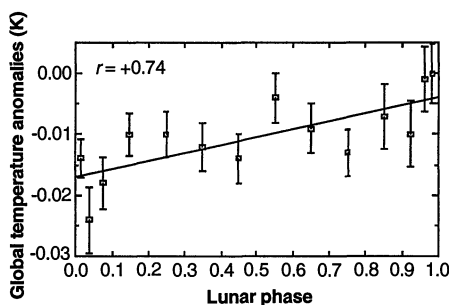


Fig. 1. Plot of averaged global temperature anomalies versus lunar phase category along with 0.95 confidence intervals for the means. The cycle of lunar phase magnitudes varies from 0.0 (new moon) to 1.0 (full moon).

values > 0.90 . The mean global temperature anomaly was -0.02 K ($n = 1129$ days) in the new moon class and 0.00 K ($n = 1066$ days) in the full moon class. A t test comparing the group means determined that the global average temperatures were significantly different ($t = 1.63$; $P = 0.05$).

3) Similarly, we divided the lunar phase data into two classes based on the planetary temperature anomalies. One class with temperature anomalies < -0.3 K had a mean lunar phase of 0.49 ($n = 518$), whereas the other class with anomalies > 0.3 K had a mean lunar phase of 0.55 ($n = 415$). A t test comparing the lunar phase averages showed that the means were significantly different ($t = 2.43$; $P = 0.01$).

4) The dominant cycles present in the daily global temperature data set may be identified with the spectral analysis program used by Ruddiman and McIntyre (23). The spectral analysis of the entire data set shows an identifiable periodicity corresponding to the lunar synodic (29.53-day) cycle (Fig. 2). A weaker cycle near 14.77 days, corresponding to a lunar half-synodic cycle, is also evident in the daily global temperature record.

The existence of an identifiable relation between lunar phase and global temperature begs the question as to its fundamental cause. Presumably the causal factor is lunar, but, as pointed out by researchers examining the relation between precipitation and lunar phase (3, 4), this cannot be demonstrated by statistical analyses alone. Other scientists who have examined the lunar influence on various climatic variables have suggested several causative linkages. For example, increased thunderstorm activity near the time of the full moon may be related to lunar distortions of Earth's magnetic tail (5). Another hypothesis advanced to explain the precipitation-lunar phase relation involves the lunar modulation of meteoritic dust (2). Others have speculated that lunar tidal

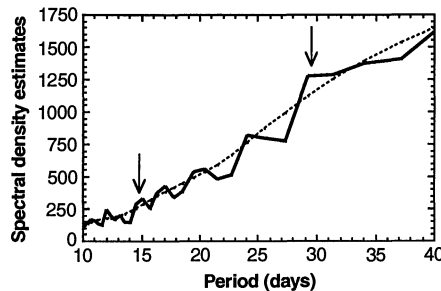


Fig. 2. Partial plot of the spectral density estimates (thick solid line) of the daily global temperature record from 3 January 1979 to 31 August 1994 at a bandwidth of 0.0281 (thin dotted line is for $P = 0.10$). Arrows indicate spectral peaks for the lunar period (29.53 days) and the synodic half-period (14.77 days).

changes could influence Earth's basic atmospheric circulation patterns, in particular, the position of the subtropical high-pressure belts (24).

Also, with respect to global temperature variations, a full moon results in an increased solar load due to the moon's reflection as well as to an increase in infrared emission from the moon's surface. The infrared flux to Earth is five orders of magnitude less than the direct flux from the sun, whereas the shortwave flux is six orders of magnitude less than the direct flux from the sun (10, 25); the 0.02 K modulation in temperature identified in this study is correspondingly five orders of magnitude less than the mean lower-tropospheric temperature. Feedback responses of global temperature to potentially lunar-related variations in other climatic parameters, such as precipitation, cloudiness, and thunderstorm activity, may also account for the lunar effect on global temperatures.

Our analyses show a significant empirical relation between lunar phase and daily planetary temperature over the past 15 years. The lunar phase appears to produce a modulation of approximately 0.03 K in the lower troposphere, with the warmest daily temperatures over a synodic month coincident with the occurrence of the full moon. The results not only confirm the suspicions of many past scientists but also suggest that the daily global temperature measurements are quite accurate. Most important, lunar influence is identified as another potential forcing mechanism to consider in the analysis of variability in the short-term, global temperature record.

REFERENCES AND NOTES

1. D. A. Bradley, M. A. Woodbury, G. W. Brier, *Science* **137**, 748 (1962).
2. E. E. Adderley and E. G. Bowen, *ibid.*, p. 749.
3. G. Brier and D. A. Bradley, *J. Atmos. Sci.* **21**, 386 (1964).
4. K. Hanson, G. A. Maul, W. McLeish, *J. Climate Appl. Meteorol.* **26**, 1358 (1987).
5. M. D. Lethbridge, *J. Geophys. Res.* **75**, 5149 (1970).
6. E. K. Bigg, *Nature* **197**, 172 (1963).
7. G. W. Brier and J. Simpson, *Q. J. R. Meteorol. Soc.* **95**, 120 (1969).
8. T. H. Carpenter, R. L. Holle, J. J. Fernandez-Partagas, *Mon. Weather Rev.* **100**, 451 (1972).
9. I. A. Lund, *J. Atmos. Sci.* **22**, 24 (1965).
10. C. H. Best, *Geophys. Res. Lett.* **21**, 2369 (1994).
11. R. W. Spencer and J. R. Christy, *Science* **247**, 1558 (1990).
12. ———, *J. Climate* **5**, 858 (1992).
13. M. R. Allen *et al.*, *Nature* **370**, 24 (1994).
14. J. R. Christy, in *Global Climate Change: Implications, Challenges, and Mitigation Measures*, S. K. Majumdar, L. S. Kalkstein, B. M. Yarnal, E. W. Miller, L. M. Rosenfeld, Eds. (Pennsylvania Academy of Science, Easton, 1992), pp. 165–178.
15. J. R. Christy and R. T. McNider, *Nature* **367**, 325 (1994).
16. J. W. Hurrell and K. E. Trenberth, *J. Climate* **5**, 1424 (1992).

17. P. D. Jones, *Geophys. Res. Lett.* **21**, 1149 (1994).
18. T. R. Karl, R. W. Knight, J. R. Christy, *J. Climate* **7**, 1144 (1994).
19. K. E. Trenberth, J. R. Christy, J. W. Hurrell, *ibid.* **5**, 1405 (1992).
20. P. D. Jones and T. M. L. Wigley, *Nature* **344**, 711 (1990).
21. J. R. Christy, R. W. Spencer, R. T. McNider, *J. Climate*, in press.
22. A. H. Gordon, *Nature* **367**, 325 (1994).
23. W. F. Ruddiman and A. McIntyre, *Science* **212**, 617 (1981).
24. R. A. Bryson, *Trans. Am. Geophys. Union* **29**, 473 (1948).
25. W. D. Sellers, *Physical Climatology* (Univ. of Chicago Press, Chicago, 1965).
26. Portions of this research were supported by NSF grant SES 9121398.

8 November 1994; accepted 11 January 1995

Conformation of Macromolecules in the Gas Phase: Use of Matrix-Assisted Laser Desorption Methods in Ion Chromatography

Gert von Helden, Thomas Wytenbach, Michael T. Bowers*

Conformational data for macromolecules in the gas phase have been obtained by the coupling of a matrix-assisted laser desorption ion source to an ion chromatograph. A series of polyethylene glycol (PEG) polymers "cationized" (converted to a cation) by sodium ions (Na^+ PEG9 to Na^+ PEG19) and a protonated neurotransmitter protein, bradykinin, were studied. Mobilities of Na^+ PEG9 to Na^+ PEG19 are reported. Detailed modeling of Na^+ PEG9 with molecular mechanics methods indicates that the lowest energy structure has the Na^+ ion "solvated" by the polymer chain with seven oxygen atoms as nearest neighbors. The agreement between the model and experiment is within 1 percent for Na^+ PEG9, Na^+ PEG13, and Na^+ PEG17, giving strong support to both the method and the deduced structures. Similar agreement was obtained in initial studies that modeled experimental data for arginine-protonated bradykinin.

Determination of the preferred conformations of large molecules traditionally has been restricted to the condensed phase, both as a means of inhibiting intramolecular motion and as a way of increasing the number density of the target molecule. For biomolecules such as proteins, the relation between conformation and activity has long been an active area of research, especially the relation between protein folding and genetic expression (1). With the advent of matrix-assisted laser desorption ionization (MALDI) (2) and electrospray ionization (ESI) (3), it has become routine to desorb molecules of nearly any size into the gas phase, where they can be examined by mass spectrometry (4). A primary focus of this work has been the determination of structural features of these molecules. For example, considerable progress has been made in determining amino acid sequences of proteins (5) and, as an adjunct to this work, the importance of metal ions as cationizing agents both for sequence studies and for investigations of their influence on peptide chemistry (6, 7).

More recently, attention has turned to conformational studies of macromolecules. For example, ESI charge distributions of select, multiply charged ions can change

with solution properties such as pH or solvent. These results were interpreted in terms of conformational changes in the biomolecules of interest (8). Another approach involves counting the labile peptide protons by isotopic exchange, because the extent of exchange is believed to correlate with the degree of folding of the protein (9). Finally, the different collision cross sections that different conformers might exhibit have been used to distinguish "larger" conformers from "smaller" conformers of multiply charged ions in triple quadrupole instruments (10).

Each of the above conformational studies used ESI and hence dealt with multiply charged ions rather than singly charged

ions. In addition, although the conclusions about the existence of different conformations were usually unambiguous, none of the methods were designed to give any detailed structural information on the various conformers observed. In this report, we describe the use of MALDI in conjunction with our recently developed ion chromatography (IC) technique (11). When combined with molecular mechanics-dynamics methods, these data provide unambiguous structural information on singly charged cationized macromolecules in the gas phase.

We investigated the gas-phase structure of various polyethylene glycol (PEG) polymers in the range PEG9 to PEG19 (that is, from 9 to 19 $-(\text{CH}_2\text{CH}_2\text{O})-$ monomer units). These are ideal systems for an initial study because they give a range of molecules whose connectivities are known and that change in a known way. Hence, the effect of chain length on conformation can be studied. A known series also provides a stringent test of the IC method as it must be able to reproduce and account for these changes without changing the molecular parameters used in modeling the system. Moreover, because PEG is cationized by Na^+ in our experiments, we can investigate the metal ion binding site (or sites) in a series of macromolecules of significant size. Finally, the distribution of PEG neutral species results in a distribution of the cationized polymers formed in the MALDI process, reducing the intensity of any one system by about an order of magnitude and providing a real test of the sensitivity of the method. The success of these experiments prompted application to biopolymers, and our initial work on the polypeptide bradykinin yielded parent ion signals an order of magnitude greater than for individual PEG systems, which made data acquisition much easier. These results, which will be discussed briefly here, will be published elsewhere (12).

Ions were made in a MALDI source built at the University of California at Santa Barbara, which is described elsewhere (13).

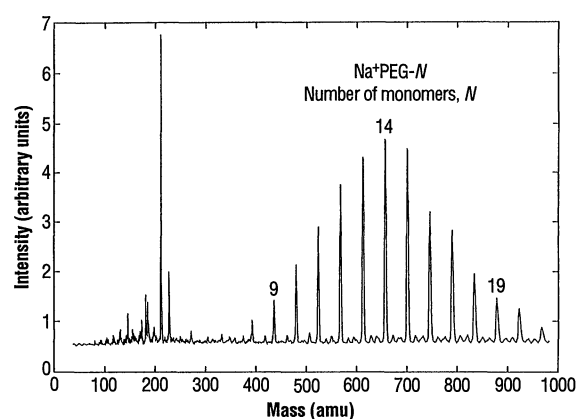


Fig. 1. A MALDI mass spectrum of a commercial PEG-600 sample present at 0.1% in a sinapinic acid matrix. All peaks below mass 300 (amu = atomic mass unit) are due to the matrix. A number of the Na^+ -cationized PEG peaks are identified.

Department of Chemistry, University of California, Santa Barbara, CA 93106, USA.

*To whom correspondence should be addressed.